Hydrogen Bonding and Solvent Structure in an Antigen−Antibody Interface. Crystal Structures and Thermodynamic Characterization of Three Fv Mutants Complexed with Lysozyme[†,#]

Barry A. Fields,[‡] Fernando A. Goldbaum,[‡,§] William Dall'Acqua,[‡] Emilio L. Malchiodi,[‡,||] Ana Cauerhff,[‡,§] Frederick P. Schwarz,[‡] Xavier Ysern,[⊥] Roberto J. Poljak,[‡] and Roy A. Mariuzza*[,‡]

Center for Advanced Research in Biotechnology, University of Maryland Biotechnology Institute and National Institute of Standards and Technology, 9600 Gudelsky Drive, Rockville, Maryland 20850, CONICET, Catedra de Inmunologia, FFYB-UBA, Junin 956, 1113 Buenos Aires, Argentina, and Center for Drug Evaluation and Research, U.S. Food and Drug Administration, 5600 Fishers Lane, Rockville, Maryland 20857

Received July 12, 1996; Revised Manuscript Received September 26, 1996[⊗]

ABSTRACT: Using site-directed mutagenesis, X-ray crystallography, and titration calorimetry, we have examined the structural and thermodynamic consequences of removing specific hydrogen bonds in an antigen−antibody interface. Crystal structures of three antibody FvD1.3 mutants, V_LTyr50Ser (V_LY50S), V_HTyr32Ala (V_HY32A), and V_HTyr101Phe (V_HY101F), bound to hen egg white lysozyme (HEL) have been determined at resolutions ranging from 1.85 to 2.10 Å. In the wild-type (WT) FvD1.3−HEL complex, the hydroxyl groups of V_LTyr50, V_HTyr32, and V_HTyr101 each form at least one hydrogen bond with the lysozyme antigen. Thermodynamic parameters for antibody−antigen association have been measured using isothermal titration calorimetry, giving equilibrium binding constants K_b (M^{-1}) of 2.6×10^7 (V_LY50S), 7.0×10^7 (V_HY32A), and 4.0×10^6 (V_HY101F). For the WT complex, K_b is 2.7×10^8 M^{-1}; thus, the affinities of the mutant Fv fragments for HEL are 10-, 4-, and 70-fold lower than that of the original antibody, respectively. In all three cases entropy compensation results in an affinity loss that would otherwise be larger. Comparison of the three mutant crystal structures with the WT structure demonstrates that the removal of direct antigen−antibody hydrogen bonds results in minimal shifts in the positions of the remaining protein atoms. These observations show that this complex is considerably tolerant, both structurally and thermodynamically, to the truncation of antibody side chains that form hydrogen bonds with the antigen. Alterations in interface solvent structure for two of the mutant complexes (V_LY50S and V_HY32A) appear to compensate for the unfavorable enthalpy changes when protein−protein interactions are removed. These changes in solvent structure, along with the increased mobility of side chains near the mutation site, probably contribute to the observed entropy compensation. For the V_HY101F complex, the nature of the large entropy compensation is not evident from a structural comparison of the WT and mutant complexes. Differences in the local structure and dynamics of the uncomplexed Fv molecules may account for the entropic discrepancy in this case.

Protein−protein recognition is essential to many biochemical processes. Factors that contribute to the structure and energetics of protein−protein interactions include hydrogen bonds, salt bridges (Chacko et al., 1995), van der Waals contacts (Ysern et al., 1994; Clackson & Wells, 1995; Chilkoti et al., 1995; Schreiber & Fersht, 1995), interface solvent networks (McPhalen & James, 1988; Bhat et al., 1994), solvent exclusion (the hydrophobic effect), and conformational changes associated with the binding reaction (Colman et al., 1987; Bhat et al., 1990, 1994). In addition to their intrinsic interest, antigen−antibody complexes represent excellent model systems for studying the structure and thermodynamics of protein−protein interactions in general. Crystallographic structures of several complexes of antibodies, or antibody fragments, bound to protein antigens are available, and the kinetic and thermodynamic binding parameters have been determined for some of these complexes. The crystal structure of the anti-hen egg white lysozyme (HEL)[1] antibody, FabD1.3, bound to HEL, shows that ~700 Å^2 of surface area is buried on both the antibody and antigen upon complex formation. As well as van der Waals contacts, hydrogen bonds that bridge antibody and antigen contribute to the binding energy and structural specificity of the complex (Amit et al., 1986; Fischman et al., 1991). Similar observations have been made for other antibody−antigen complexes including those with the fol-

[†] This work was supported by NIH Grant GM52801 (R.A.M.) and the Human Frontiers Science Program (R.J.P.).

[#] Atomic coordinates for the structures discussed herein have been deposited with the Brookhaven Protein Data Bank as entries 1KIP, 1KIQ, and 1KIR.

* Author to whom correspondence should be addressed. Tel: (301) 738-6243. FAX: (301) 738-6255. E-mail: mariuzza@indigo2.carb.nist.gov.

[‡] University of Maryland Biotechnology Institute and National Institute of Standards and Technology.

[§] Present address: CONICET, Catedra de Inmunologia, FFYB-UBA, Junin 956, 1113 Buenos Aires, Argentina.

[||] CONICET.

[⊥] U.S. Food and Drug Administration.

[⊗] Abstract published in *Advance ACS Abstracts,* November 1, 1996.

[1] Abbreviations: HEL, hen egg white lysozyme; V_L, light chain variable domain; V_H, heavy chain variable domain; Fv, variable domain fragment ($V_L + V_H$); Fab, antigen binding fragment; PBS, phosphate-buffered saline; K_b, equilibrium binding constant; CDR, complementarity determining region; WT, wild type; rms, root mean square.

S0006-2960(96)01709-6 CCC: $12.00

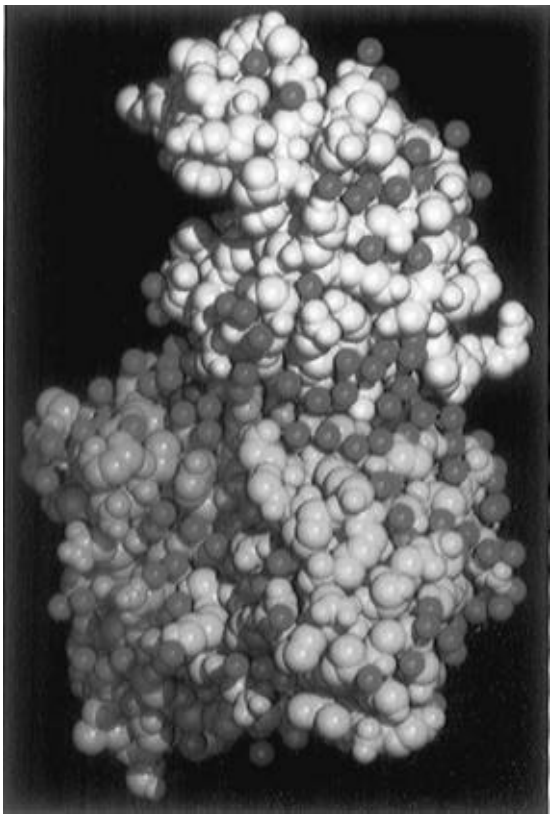

FIGURE 1: Space-filling model of the FvD1.3−HEL complex. The interface between FvD1.3 V_L (yellow), V_H (blue), and lysozyme (white) is highly solvated (water oxygen atoms drawn as green spheres). V_HTyr32 and V_LTyr50, in red, are partially visible on the left and right side of the interface, respectively. V_HTyr101 is buried in the interface and is obscured by other atoms. Drawn with QUANTA.

lowing protein antigens: neuraminidase (Colman et al., 1987; Tulip et al., 1992a,b; Malby et al., 1994), histidine-containing protein (Prasad et al., 1993), staphylococcal nuclease (Bossart-Whitaker et al., 1995), influenza hemagglutinin (Bizebard et al., 1995), and other antibody−lysozyme complexes (Sheriff et al., 1987; Padlan et al., 1989; Chitarra et al., 1993; Braden et al., 1994, 1996; Lescar et al., 1995). Since both the number and the local environment of antigen−antibody hydrogen bonds vary from complex to complex, the contribution of individual hydrogen bonds to antigen−antibody complex formation is a matter of great interest. It is still not clear how the strength of hydrogen bonds in a protein−protein interface varies with the relative geometry of the interacting groups, the local chemical environment, and how these hydrogen bonds can influence the dynamic behavior of neighboring groups.

With the aim of increasing our structural understanding of antigen−antibody energetics, we have determined the crystal structures of three mutants of the Fv fragment (a heterodimer consisting of only the light and heavy chain variable domains, V_L and V_H) of D1.3 bound to its protein antigen HEL. These mutants were designed to disrupt hydrogen bonds between the antigen and antibody. The structure of the WT FvD1.3−HEL complex is shown in Figure 1. In the present study, we have mutated three FvD1.3 tyrosine residues that form hydrogen bonds with HEL. These hydrogen bonds are shown in Figure 2. The WT FvD1.3 fragment binds HEL with an affinity ($K_b = 2.7 \times 10^8$ M^{-1}) equal to that of the Fab and the intact

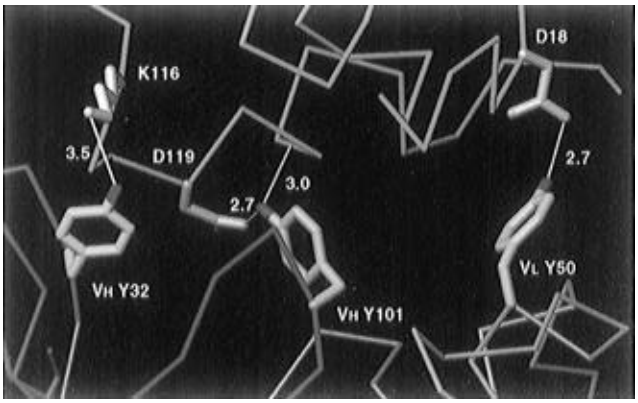

FIGURE 2: Hydrogen bonds between lysozyme and FvD1.3 tyrosine residues V_LTyr50, V_HTyr32, and V_HTyr101. The orientation is similar to that for Figure 1.

immunoglobulin (Bhat et al., 1994). This reaction has been shown to be enthalpically driven ($\Delta H = -90$ kJ·mol^{-1}) with an opposing entropic term ($T\Delta S = -42$ kJ·mol^{-1}). The crystal structure of FvD1.3 bound to HEL, determined at 1.8 Å resolution (Bhat et al., 1994), reveals a large number of water molecules in the Fv−HEL interface that probably contribute significantly to the enthalpy of complex formation (Figure 1). Calorimetric measurements of FvD1.3-HEL binding at reduced water concentration support this hypothesis (Goldbaum et al., 1996). These experiments involved addition of cosolutes such as glycerol, ethanol, dioxane, and methanol in order to reduce the effective water activity. In accord with the concept that the interface water molecules are important for complex stability, it was found that the enthalpies of reaction as well as the association constants decreased with decreasing water activity. The fact that many water molecules reside in the protein−protein interface also aids rationalization of the opposing entropic term. Interface water molecules that are not ejected into the bulk solvent upon binding cannot contribute to the hydrophobic effect. Moreover, interface water molecules that are "recruited" from the bulk solvent during the binding reaction provide a negative contribution to the hydrophobic effect. Thus, in addition to protein−protein hydrogen bonds, we were also interested in observing how this network of interface water molecules responds to the substitution of interface amino acids. The thermodynamic consequences of the mutations were analyzed using isothermal titration calorimetry which enabled determination of K_b, $\Delta H°$, and $T\Delta S$. We will address how alterations in the following factors induced by site-directed mutagenesis affect the structure and energetics of protein−protein complex formation in this system: (i) hydrogen bonding, (ii) van der Waals contacts, (iii) conformation of antigen and antibody, (iv) mobility of antigen and antibody, and (v) solvent structure.

MATERIALS AND METHODS

Reagents. All chemicals were of analytical grade. Restriction enzymes and DNA-modifying enzymes were purchased from New England Biolabs, Inc. (Beverly, MA). Radiolabeled [^{35}S]dATP was obtained from Amersham Corp. Oligonucleotides were synthesized on a 380B DNA synthesizer (Applied Biosystems, Foster City, CA).

Site-Directed Mutagenesis. For mutagenesis of the D1.3 V_L region, a 441 bp *Eco*RI fragment was transferred from the pUC19-based bacterial expression vector pSW1-VHD1.3-

VKD1.3 described by Ward et al. (1989) to M13mp19. For mutagenesis of the V_H region, a 477 bp *Hin*dIII fragment from pSW1-VHD1.3-VKD1.3 was subcloned in M13mp19. Oligonucleotide site-directed mutagenesis was carried out as described (Kunkel et al., 1987) with a MutaGene M13 in vitro mutagenesis kit (Bio-Rad, Richmond, CA) to introduce the V_LY50S, V_HY32A, and V_HY101F mutations. All mutations were confirmed by the dideoxynucleotide sequencing method (Sanger et al., 1977) using a Sequenase version 2.0 kit (USB, Cleveland, OH). For religation into the FvD1.3 expression vector, the mutated V_L gene was restricted with *Eco*RI and the V_H gene with *Hin*dIII.

Expression and Purification of Fv fragments. All three mutants were prepared from the culture supernatants of transformed *Escherichia coli* BMH 71-18 cells as described (Ward et al., 1989; Ysern et al., 1994). Briefly, recombinant clones were resuspended in 10 mL of Terrific broth (Tartof & Hobbs, 1987) containing 100 $\mu g \cdot mL^{-1}$ ampicillin and 1% (w/v) glucose to repress FvD1.3 expression. The cultures were incubated at 37 °C under agitation to an absorbance of 1.0 at 600 nm. The cells were then pelleted by centrifugation, washed twice with medium, and resuspended in 500 mL of Terrific broth containing 100 $\mu g \cdot mL^{-1}$ ampicillin and 0.1% (w/v) glucose. This glucose concentration is high enough for cells to grow normally, yet low enough to permit efficient induction following its depletion from the medium as a result of bacterial metabolism. The cultures were grown at 37 °C to an absorbance of 1.0, and isopropyl β-thiogalactoside (Gold Biotechnology, St. Louis, MO) was added to a final concentration of 1.0 mM. After further incubation at 37 °C for 4 h, the bacteria were pelleted and the FvD1.3 mutants were affinity purified from the supernatants using the anti-D1.3 monoclonal antibody E5.2 (Ysern et al., 1994; Fields et al., 1995) coupled to Sepharose 4B (about 7.5 mL/L of culture). Columns were washed with 100 volumes of phosphate-buffered saline (PBS), pH 7.4, and eluted with 50 mM diethylamine, pH 12. Fractions were immediately neutralized with 1.0 M Tris-HCl, pH 7.0, and concentrated using Centricon 3000 spin columns (Amicon, Beverly, MA). Further purification of FvD1.3 mutants was carried out by size exclusion chromatography on a ZORBAX GF-250 column (DuPont) in 0.2 M sodium phosphate buffer, pH 7.4 (Boulot et al., 1990). Final yields were typically 0.5−1.0 mg/L of culture.

Crystallography. A small molar excess of HEL (Boehringer-Mannheim, Indianapolis, IN) was added to purified FvD1.3 mutants, and the complexes were crystallized in hanging drops by vapor diffusion. Crystallization conditions were similar to those used for the WT Fv−HEL complex (Boulot et al., 1990): 15−18% (w/v) poly(ethylene glycol) 8000 (Sigma) and 0.1 M potassium phosphate, pH 6.0−6.5. Macroseeding (Thaller et al., 1981) in hanging drops was used to obtain crystals with dimensions up to 0.4 mm × 0.2 mm × 0.1 mm. X-ray diffraction data were recorded on a Siemens area detector mounted on either a Siemens or a Rigaku rotating-anode X-ray generator. Data were indexed, integrated, and reduced using XENGEN version 2.0 (Howard et al., 1987). All complexes crystallized isomorphously with the WT complex in space group *C*2. Unit cell dimensions are shown in Table 1. Each structure was refined using X-PLOR (Brünger, 1992) starting from the WT complex (PDB accession code 1VFB) with all water molecules deleted. The first step in each refinement consisted of rigid-body refinement, treating each of the three polypeptide chains as an independent rigid unit. Next, an $F_{o(mutant)} - F_{c(WT)}$ difference electron density map was calculated and inspected in order to confirm the mutation. Refinement then consisted of (i) modeling the mutation into the electron density, (ii) an additional stage of rigid-body refinement, (iii) one stage of simulated annealing starting at a temperature of 3000 K, and (iv) iterative cycles of positional refinement, temperature factor refinement, and inspection of electron density maps (with coefficients $2F_o - F_c$ and $F_o - F_c$) including location of ordered solvent molecules. An electron density difference peak was modeled as a water molecule if it was higher than 3.5σ, made contact with at least one potential hydrogen bond donor or acceptor in the range 2.4−3.4 Å, and remained in electron density (1σ, $2F_o - F_c$) after subsequent refinement. The solvent structure in the WT FvD1.3−HEL structure was not used to assist location of water molecules in the mutant complexes.

Table 1: Crystallographic Data Processing and Refinement Statistics for FvD1.3−HEL Complexes

	V_LY50S	V_HY32A	V_HY101F
data processing			
cell parameters			
a (Å)	129.2	129.2	129.8
b (Å)	60.5	60.4	60.4
c (Å)	56.8	56.6	56.8
β (deg)	119.0	119.1	119.1
observations	47313	49442	84404
unique reflections	21066	20023	33574
redundancy	2.2	2.5	2.5
R_{merge}[a]	0.082	0.086	0.083
refinement			
data range (Å)	7.0−2.00	7.0−2.10	6.0−1.85
reflections	16783	15354	23568
completeness (%)[b]	66, 41	70, 30	74, 37
no. of waters	142	116	166
rmsd bond lengths (Å)	0.016	0.015	0.016
rmsd bond angles (deg)	1.91	1.93	1.86
mean *B*-factors[c] (Å^2)			
V_L	24	19	19
V_H	27	23	24
HEL	33	31	30
water	35	33	37
R-factor[d]	0.167	0.162	0.181

[a] $R_{merge} = \sum|I(k) - \langle I\rangle|/\sum I(k)$, where $I(k)$ and $\langle I\rangle$ are the *k*th individual and mean values of the intensity of a reflection, respectively. [b] First and second values correspond to completeness in the entire data range and in the highest resolution 0.1 Å shell (e.g., 1.95−1.85), respectively. [c] Mean *B*-factors (Å^2) for the WT structure are 22 (V_L), 26 (V_H), 32 (HEL), and 43 (water). [d] *R*-factor $= \sum|F_o - F_c|/\sum|F_o|$, where F_o and F_c are the observed and calculated structure factor amplitudes, respectively.

Titration Calorimetry. Affinity-purified FvD1.3 mutants were dialyzed against PBS prior to calorimetry. A phosphate buffer was used to minimize effects due to any exchange of protons upon binding to HEL. In a typical experiment, 5 μL aliquots of a 1.00 mM HEL solution were titrated into a 0.05 mM Fv solution at 25 °C, and the evolved heats were measured with a Microcal Omega titration calorimeter as described (Wiseman et al., 1989; Schwarz et al., 1993, 1995; Bhat et al., 1994). The titrations were continued beyond saturation of the antibody-combining sites to determine any heat contributions from dilution of the HEL solution upon its addition to the antibody solution. The heats below the saturation point were accordingly corrected for any heat of dilution of the HEL solution. Protein concentrations were calculated using 1% extinction coefficients at 280 nm of 1.50

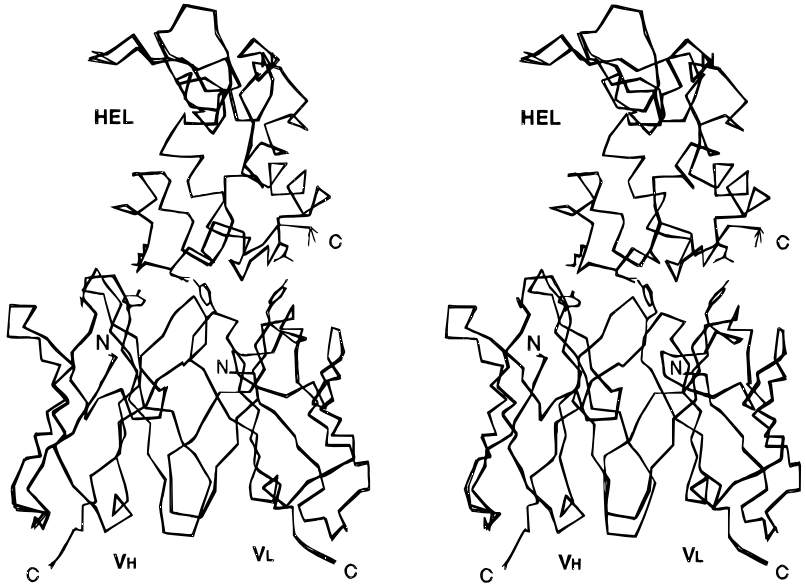

FIGURE 3: Superposition of four FvD1.3−HEL structures: WT, V_LTyr50Ser, V_HTyr32Ala, and V_HTyr101Phe. C^α atoms plus the side chains of the relevant interacting residues are shown in stereo. Note the large variation in the position of the HEL C-terminus which has high temperature factors and weak electron density. See also Table 2.

Table 2: rms Deviation (Å) of All C^α Atoms after Least-Squares Superposition of FvD1.3−HEL Structures

	V_LY50S	V_HY32A	V_HY101F
WT	0.22	0.21	0.22
V_LY50S		0.20	0.23
V_HY32A			0.19

and 2.62 for Fv and HEL, respectively. Values for ΔH_b and K_b were determined from a fit of the heat exchanged per injection as a function of the amount of injecting titrant utilizing the software program Origin (Microcal Inc.). This software is based on the analysis of the amount of heat exchanged during the titration as described by Wiseman et al. (1989). The binding entropy contribution, $T\Delta S_b$, was calculated from $\Delta G_b^\circ = \Delta H_b - T\Delta S_b$, where $\Delta G_b^\circ = -RT \ln K_b$. Control titrations performed in 0.15 M NaCl, 0.01 M Tris-HCl, pH 7.2, gave the same binding enthalpies, within experimental error, indicating the absence of significant proton exchange in the Fv−HEL reactions.

RESULTS

Crystallographic data for the mutant complexes are shown in Table 1. The maximum resolution of the X-ray data used in the refinements ranges from 1.85 to 2.10 Å, and the *R*-factors of the refined structures range from 0.162 to 0.181. As shown in Figure 3 and Table 2, the positions of C^α atoms in the mutant structures are very similar to those of the WT complex, indicating that the substitutions in the complementarity determining regions (CDRs) do not significantly affect the conformations of these loops or the relative orientations of V_L, V_H, and HEL in the complex. This observation is consistent with previous crystallographic studies of antibody−antigen complexes with interface mutations (Tulip et al., 1992b; Ysern et al., 1994; Chacko et al., 1995). Electron density difference maps calculated at the start of refinement are consistent with the amino acid substitutions in each mutant complex (Figure 4). The calorimetric data for the mutant complexes are shown in Table 3. Binding constants for FvD1.3−HEL association (K_b) range from 4.0×10^6 to 7.0×10^7 M^{-1}.

Structure and Calorimetry of the V_LY50S Complex. The binding constant of V_LY50S-HEL is 2.6×10^7 M^{-1}, which is 10-fold less than that of the WT complex. This affinity loss corresponds to a $\Delta\Delta G_b^\circ$ of 6.1 kJ·mol^{-1} in which an unfavorable $\Delta\Delta H$ of 8.8 kJ·mol^{-1} is partially compensated by a favorable $\Delta(T\Delta S)$ of 2.7 kJ·mol^{-1} (Table 3). Tyr50 of the antibody V_L domain makes one direct hydrogen bond to an Asp side chain of the lysozyme antigen (FvD1.3 Tyr50 $O^\eta \cdots O^{\delta 2}$ $Asp18_{HEL}$, 2.7 Å) and also participates in the interface water network. When V_LTyr50 is mutated to Ser, this direct hydrogen bond is replaced by solvent-mediated interactions to the HEL side chain (V_LSer50 $O^\gamma \cdots H_2O \cdots H_2O \cdots O^{\delta 1}$ $Asp18_{HEL}$). These two bridging water molecules occupy some of the volume that was taken up by the V_LTyr50 side chain in the WT structure (Figure 5A). Several neighboring water molecules are in positions that correspond closely to those of the WT structure while others are not observed in the crystal structure probably because of the lower resolution of this structure compared to the WT crystal structure. Conformational changes in the vicinity of the mutation are largest at HEL side chains Asp18 and Asn19—the residues that are in closest contact to V_LTyr50 of FvD1.3 in the WT structure (Figure 5A). The largest difference in atomic positions (1.1 Å) occurs at Asp18 $O^{\delta 2}$. In addition, the temperature factors of these side chains increase when V_LTyr50 is replaced with Ser (Table 4). As well as losing a direct hydrogen bond to the lysozyme antigen, several van der Waals contacts are also lost, which should contribute to the observed unfavorable enthalpy change (Table 5).

Structure and Calorimetry of the V_HY32A Complex. The side chain of V_HTyr32 makes a long potential hydrogen bond (3.5 Å) with the side chain of lysozyme residue Lys116 and, like V_LTyr50, is involved in a solvent network that bridges antigen and antibody. Mutation to Ala disrupts the solvent network but does not affect the conformation or temperature factors of $Lys116_{HEL}$ (Figure 5B, Table 4). The V_HY32A mutant binds lysozyme with only about 4-fold lower affinity than that of the WT Fv. In this case the large $\Delta\Delta H$ (17.9 kJ·mol^{-1}) is almost fully compensated by the entropic term resulting in the small decrease in affinity (Table 3). As for

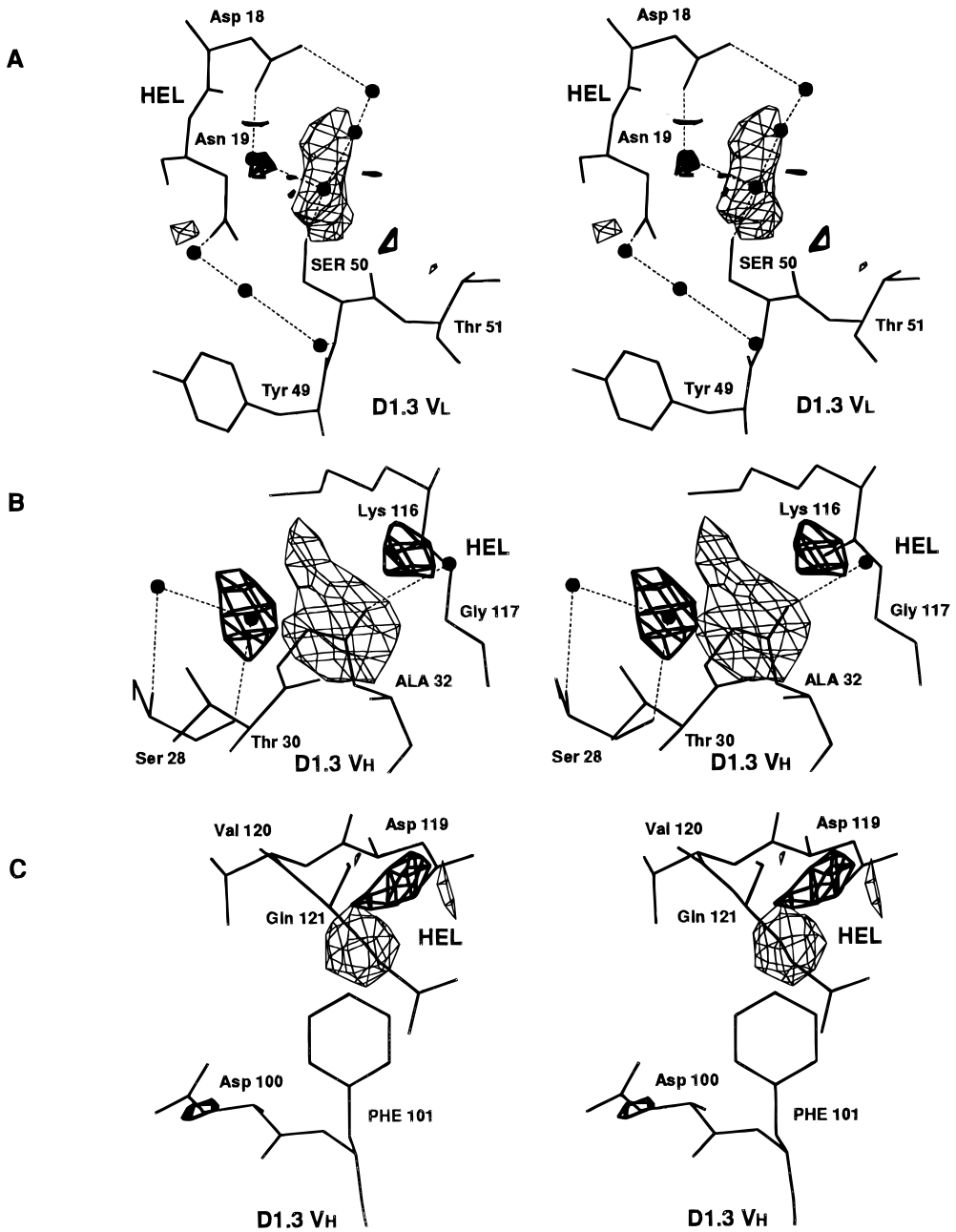

FIGURE 4: Stereo electron density difference maps calculated at the start of refinement superposed on the final refined structures: (A) V_LTyr50Ser, (B) V_HTyr32Ala, and (C) V_HTyr101Phe. Contours are drawn at $+3\sigma$ (thick lines) and -3σ (thin lines).

Table 3: Calorimetric Data for FvD1.3−HEL Complex Formation[a]

mutant	K_b (M^{-1})	$\Delta\Delta G°$ (kJ·mol^{-1})	$\Delta\Delta H$ (kJ·mol^{-1})	$\Delta(T\Delta S)$ (kJ·mol^{-1}·K^{-1})
wild type[b]	$(2.7 \pm 1.0) \times 10^8$	0.0	0.0	0.0
V_LY50S	$(2.6 \pm 0.4) \times 10^7$	6.1 ± 0.1	8.8 ± 0.2	2.7 ± 0.1
V_HY32A	$(7.0 \pm 1.8) \times 10^7$	3.6 ± 0.1	17.9 ± 0.8	14.3 ± 0.7
V_HY101F	$(4.0 \pm 1.3) \times 10^6$	10.9 ± 0.2	31.3 ± 0.6	20.4 ± 1.4

[a] $\Delta\Delta X = \Delta X_{mutant} - \Delta X_{WT}$, where $X = G$ or H. $\Delta(T\Delta S) = T\Delta S_{mutant} - T\Delta S_{WT}$. [b] From Bhat et al. (1994).

the V_LY50S mutant, a rearrangement in the local solvent structure is clear. However, in contrast with V_LY50S, only one van der Waals contact is lost along with the long hydrogen bond (Table 5). There are two side chains in the vicinity of the mutation whose mobilities are affected by the V_HY32A mutation. When V_HTyr32 is truncated to Ala, V_HArg99 loses stabilizing contacts with V_HTyr32 and becomes more mobile, as indicated by an increase in the mean temperature factor of side chain atoms from 28 to 40 Å^2 (Table 4). A conformational change in V_HArg99, resulting in a maximum atomic displacement of 1.1 Å from the WT structure, accompanies the temperature factor increase. In contrast, the mean temperature factor of a neighboring side chain, V_HPhe27, decreases (from 16 to 9 Å^2) while the shifts in atomic positions for this side chain are smaller (<0.5 Å).

Structure and Calorimetry of the V_HY101F Complex. Tyr101 of D1.3 V_H is situated near the center of the Fv−HEL interface and makes two hydrogen bonds with HEL: V_HTyr101 $O^{\eta}\cdots O^{\delta 1}$ $Asp119_{HEL}$ (2.7 Å) and V_HTyr101 $O^{\eta}\cdots N$ $Gln121_{HEL}$ (3.0 Å). The effective substitution of the Tyr hydroxyl group by a hydrogen atom to give the Phe mutant results in small local atomic shifts. The largest atomic displacement (0.5 Å) in the interface compared to WT occurs at $Asp119_{HEL}$ $O^{\delta 1}$—an atom involved in one of the above-

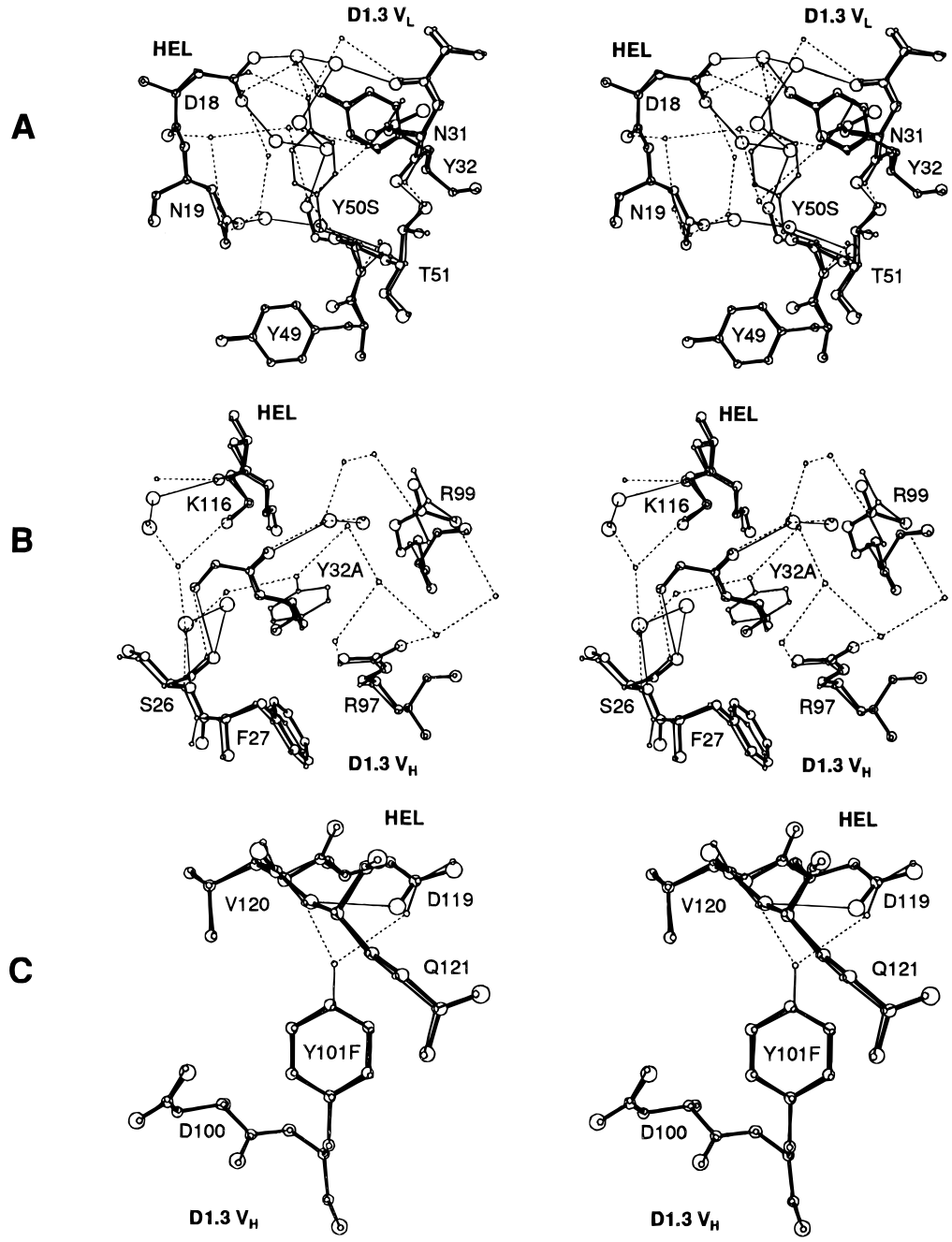

FIGURE 5: Stereo diagrams of the mutant structures (thick bonds, large atoms, continuous hydrogen bonds) superposed on the WT structure (thin bonds, small atoms, dashed hydrogen bonds): (A) V_LTyr50Ser, (B) V_HTyr32Ala, and (C) V_HTyr101Phe.

mentioned hydrogen bonds. In contrast to the other mutants, there are no increases in temperature factors for atoms in the vicinity of the mutation (Table 4). The calorimetric data indicate that the unfavorable enthalpy change resulting from the loss of two interface hydrogen bonds is strongly compensated by a favorable entropy change (Table 3). This complex exhibits the largest $\Delta\Delta H$, 31 kJ·mol^{-1}, and the largest $\Delta(T\Delta S)$, 20 kJ·mol^{-1}, of the three mutant complexes. It is important to note that there is no space for a water molecule to insert into the interface when the OH group of Tyr101 is replaced by H. Significantly, the structure shows that the side chain of $Asp119_{HEL}$ is not left with its hydrogen-bonding potential unsatisfied in the mutant. Instead, $Asp119_{HEL}$ forms an intramolecular hydrogen bond with $Gln121_{HEL}$ N (3.2 Å). In the WT structure, the corresponding distance is 3.8 Å, which is too long to be a hydrogen bond.

DISCUSSION

The FvD1.3 system is particularly suitable for the study of protein−protein complex energetics and structure. High-resolution (1.8 Å) crystal structures are known for FvD1.3 both in the free state and bound to its specific antigen HEL (Bhat et al., 1994). Also, the thermodynamics of the Fv−HEL association reaction have been analyzed using isothermal titration calorimetry (Bhat et al., 1994). The availability of high-resolution crystal structures of mutant Fv−HEL complexes enables the quantitation of small, as well as large, structural changes induced by the mutation. An analysis of the precision of the crystal structures, as presented below, sets limits for significance levels pertaining to changes in atomic positions.

Precision of Crystal Structures. Luzzati plots (Luzzati, 1952) for each of the refinements (data not shown) give mean

Table 4: Mean Temperature Factors (Å^2) for Side Chains at the Mutation Sites

residue	WT	V_LY50S	V_HY32A	V_HY101F
V_LTyr49	18	20		
V_L50	16	24		
V_LThr51	14	19		
Asp18$_{HEL}$	24	35		
Asn19$_{HEL}$	19	38		
V_HPhe27	16		9	
V_H32	19		13	
V_HArg99	28		40	
Lys116$_{HEL}$	24		25	
AspV_H100	12			10
V_H101	13			12
ArgV_H102	16			11
Ser24$_{HEL}$	14			13
Asp119$_{HEL}$	17			16
Val120$_{HEL}$	13			10
Gln121$_{HEL}$	12			11

Table 5: Contacts Made to Lysozyme by FvD1.3 Residues V_L50, V_H32, and V_H101 in the WT and Mutant Complexes

WT complex				mutant complexes			
V_LTyr50 atom	HEL atom	residue	distance[a] (Å)	Ser50 atom	HEL atom	residue	distance (Å)
$C^{\delta 2}$	C^{β}	Asn19	3.8	C^{β}	C^{γ}	Asn19	3.8
$C^{\delta 2}$	C^{γ}	Asn19	3.7	C^{β}	$O^{\delta 1}$	Asn19	3.6
$C^{\delta 2}$	$N^{\delta 2}$	Asn19	3.7	O^{γ}	C^{γ}	Asn19	3.5
$C^{\epsilon 2}$	C^{γ}	Asp18	4.1	O^{γ}	$O^{\delta 1}$	Asn19	3.4
$C^{\epsilon 2}$	$O^{\delta 2}$	Asp18	3.7				
$C^{\epsilon 2}$	C^{β}	Asn19	4.0				
C^{ζ}	C^{γ}	Asp18	4.0				
C^{ζ}	$O^{\delta 1}$	Asp18	3.7				
C^{ζ}	$O^{\delta 2}$	Asp18	3.6				
O^{η}	C^{γ}	Asp18	3.4				
O^{η}	$O^{\delta 1}$	Asp18	3.2				
O^{η}	$O^{\delta 2}$	Asp18	2.7[b]				

WT complex				mutant complexes			
V_HTyr32 atom	HEL atom	residue	distance (Å)	Ala32 atom	HEL atom	residue	distance (Å)
C^{ζ}	C^{ϵ}	Lys116	4.0	no contacts from Ala32 to HEL			
O^{η}	N^{ζ}	Lys116	3.5[b]				

WT complex				mutant complexes			
V_HTyr101 atom	HEL atom	residue	distance (Å)	Phe101 atom	HEL atom	residue	distance (Å)
$C^{\epsilon 1}$	$C^{\gamma 2}$	Val120	3.8	$C^{\delta 1}$	O^{γ}	Ser24	3.7
$C^{\epsilon 1}$	C^{β}	Gln121	4.1	$C^{\epsilon 1}$	O^{γ}	Ser24	3.7
$C^{\epsilon 2}$	C^{β}	Gln121	3.9	$C^{\epsilon 1}$	$C^{\gamma 2}$	Val120	3.7
C^{ζ}	$O^{\delta 1}$	Asp119	3.7	$C^{\epsilon 1}$	C^{β}	Gln121	4.1
C^{ζ}	C^{β}	Gln121	3.5	$C^{\epsilon 2}$	C^{β}	Gln121	3.8
O^{η}	C^{α}	Asp119	3.4	C^{ζ}	$O^{\delta 1}$	Asp119	3.6
O^{η}	C^{γ}	Asp119	3.7	C^{ζ}	N	Gln121	3.7
O^{η}	$O^{\delta 1}$	Asp119	2.7[b]	C^{ζ}	C^{α}	Gln121	4.1
O^{η}	C	Asp119	3.4	C^{ζ}	C^{β}	Gln121	3.4
O^{η}	N	Val120	3.2				
O^{η}	N	Gln121	3.0[b]				
O^{η}	C^{β}	Gln121	3.2				

[a] Maximum contact distances are as follows (in Å): C−C, 4.1; C−N, 3.8; C−O, 3.7; O−O, 3.4; O−N, 3.5; N−N, 3.5. [b] Hydrogen bond (see also Table 6).

errors in atomic positions of 0.25 Å (V_LY50S and V_HY32A) and 0.22 Å (V_HY101F). These values agree closely with the rms deviations in C^{α} positions after superposition of the mutant and WT complexes (Table 2). Global estimates of precision, such as the Luzzati analysis, do not provide information about the precision of specific interactions.

Table 6: Interface Hydrogen Bond Lengths, Standard Deviations, and Ranges, Calculated from Seven FvD1.3−HEL Crystal Structures[a]

D1.3 atom	HEL atom	WT distance	mean	SD[b]	range
V_L					
His30 $N^{\delta 1}$	O^{T} Leu129	3.38	5.82[c]	1.85	5.56
Tyr50 O^{η}	$O^{\delta 2}$ Asp18	2.74	2.71	0.15	0.44
Thr53 $O^{\gamma 1}$	$N^{\delta 2}$ Asn19	2.80	2.91	0.08	0.27
Phe91 O	$N^{\epsilon 2}$Gln121	2.82	2.84	0.07	0.18
Ser93 N	$O^{\epsilon 1}$ Gln121	2.89	2.88	0.07	0.22
V_H					
Tyr32 O^{η}	N^{ζ} Lys116	3.47	3.34	0.10	0.33
Gly53 N	O Gly117	2.82	2.79	0.11	0.36
Arg99 $N^{\eta 1}$	O Gly102	2.68	2.87	0.26	0.81
Asp100 $O^{\delta 1}$	N Ser24	2.91	2.87	0.05	0.13
Asp100 $O^{\delta 2}$	O^{γ} Ser24	2.84	2.85	0.09	0.25
Asp100 $O^{\delta 2}$	$N^{\delta 2}$ Asn27	3.08	3.19	0.07	0.22
Tyr101 O^{η}	$O^{\delta 1}$ Asp119	2.70	2.54	0.08	0.28
Tyr101 O^{η}	N Gln121	3.04	3.06	0.14	0.39
Arg102 $N^{\eta 2}$	O Gly22	2.82	2.89	0.09	0.29

[a] All values in Å. These 14 interface hydrogen bonds were selected from the WT structure according to the following criteria: (i) donor−acceptor distance ≤3.5 Å and (ii) angles at donor and acceptor atoms >90°. [b] Standard deviation. [c] See text for discussion.

Individual errors may differ greatly from the overall estimate depending on, for example, the local order and dynamics, as indicated by temperature factors. In this study, the availability of refined crystal structures of several single-site mutants permits an analysis of the precision of specific interactions. Ignoring localized structural differences due to the effects of the mutations, we will assume, for statistical purposes, that each mutant structure represents an independent determination of the WT structure. It is then possible, for example, to calculate standard deviations of individual hydrogen bond lengths and van der Waals contact distances in the antibody−antigen interface and thus evaluate whether a particular structural change is significant. The seven structures used to obtain the values for the 14 interface hydrogen bonds shown in Table 6 are the WT complex (Bhat et al., 1994), the V_LTrp92Asp complex (Ysern et al., 1994), the three complexes presented here, and two unpublished mutant complexes (V_LPhe91Leu, 1.85 Å resolution, R = 0.17, and V_HAsn56Ala, 1.83 Å resolution, R = 0.16). Nine of these hydrogen bonds have standard deviations ≤0.10 Å (Table 6). The smallest standard deviation for an interface hydrogen bond length, 0.05 Å, occurs at residues with below-average temperature factors, namely, V_HAsp100 (B_{mean} = 12 Å^2) and Ser24$_{HEL}$ (B_{mean} = 14 Å^2). In striking contrast, an interaction with the C-terminus of HEL that was defined as a hydrogen bond in the WT structure, V_LHis30 $N^{\delta 1}\cdots O^{T}$ Leu129$_{HEL}$, varies dramatically in the refined mutant structures. It is evident from the high temperature factors of Leu129$_{HEL}$ (B_{mean} = 55 Å^2), its poor electron density in all structures, and its variability in conformation (see Figure 3) that any stabilizing interaction with D1.3 is transient at best. With regard to the variation of hydrogen bond lengths in the interface, this analysis indicates that the V_HTyr32 $O^{\eta}\cdots N^{\zeta}$ Lys116$_{HEL}$ interaction is relatively long while the V_HTyr101 $O^{\eta}\cdots O^{\delta 1}$ Asp119$_{HEL}$ interaction is relatively short (Table 6). In view of the standard deviations and ranges shown in Table 6, analogous statements for the remaining intermediate hydrogen bonds cannot be made with confidence.

Interface Solvent and Hydrogen Bonds. Previous studies on the FvD1.3−HEL complex have supported the concept

that solvent associated with the protein−protein interface contributes to the stability of the complex (Bhat et al., 1994; Goldbaum et al., 1996). The high-resolution crystal structure of FvD1.3−HEL shows a large number of water molecules in the interface that provide bridging hydrogen bonds and occupy what could otherwise be destabilizing voids in the interface (Figure 1). The plasticity of part of this network was illustrated in the crystal structure of an FvD1.3−HEL complex with V_LTrp92 substituted for Asp (Ysern et al., 1994). In that study, truncation of the V_LTrp92 side chain left space which was filled by two water molecules. Other water molecules in the vicinity of the mutation adjusted positions slightly, presumably to optimize hydrogen bonds and van der Waals contacts with the void-filling water molecules.

Two of the structures presented here, V_LY50S and V_HY32A, bound to HEL, also exhibit alterations in local solvent structure compared to WT. In both cases the solvent rearrangements are localized, and their effects do not extend far beyond the vicinity of the mutation. In V_LY50S, the direct hydrogen bond to HEL in the WT structure is lost and replaced by solvent-mediated interactions (Figure 5A). A bridging water molecule substituting for a direct hydrogen bond was observed in an antibody−trisaccharide system (Bundle et al., 1994; Zdanov et al., 1994). Based on geometry criteria, namely, the hydrogen bond donor−acceptor distance and the relative orientation of the interacting groups, the V_LY50S hydrogen bond with HEL would be classified as "strong". However, $\Delta\Delta H$ for V_LY50S compared to WT is only 9 kJ·mol^{-1}. Furthermore, as shown in Table 5, several van der Waals contacts are lost along with the hydrogen bond when V_LTyr50 is substituted for Ser. Based on our analysis of the contribution of van der Waals contacts by V_LTrp92 (Ysern et al., 1994), the lost contacts of Tyr50 could provide an additional ∼8 kJ·mol^{-1}.

As noted previously, Tyr50 is also involved in hydrogen-bonding interactions with the interface water network. Thus, Tyr50 interacts with HEL through a direct hydrogen bond, several van der Waals contacts, and a solvent network and would therefore appear to be energetically important. There are several ways to explain the apparently small difference in enthalpy between WT and V_LY50S: (i) the new bridging solvent in the Y50S complex provides most of the stabilizing enthalpy, (ii) the Tyr50 hydrogen bond and/or van der Waals contacts contribute much less to the enthalpy of the WT complex than estimated, (iii) the energetics of the unbound Fv molecules differ substantially, or (iv) a combination of these. The following discussion of the V_HY32A and V_HY101F complexes supports the view that localized bridging solvent can make a significant enthalpic contribution.

The V_HTyr32 $O^{\eta}\cdots N^{\zeta}$ $Lys116_{HEL}$ separation of 3.5 Å would classify this interaction as a relatively weaker hydrogen bond compared to the above-mentioned V_LTyr50 interaction (Table 6). In contrast to the situation for V_LY50S, the $\Delta\Delta H$ for V_HY32A compared to WT is large (18 kJ·mol^{-1})—a value which may be expected to correspond to a strong hydrogen bond. In this case, however, Tyr32 is also involved in a bridging solvent network which is completely lost when Tyr is replaced by Ala and is not compensated by new bridging water interactions. A new water molecule that occupies some of the space taken up by the Tyr ring in the WT structure is too distant from HEL to act as a bridge. Thus, a possible explanation for the large $\Delta\Delta H$ despite the apparently weak hydrogen bond is that the existing solvent network in the WT complex makes a sizable contribution to ΔH. This hypothesis could be tested by substitution of a residue other than Ala in place of Tyr which might preserve certain elements of the WT solvent network.

Compared to the previous two mutants, an analysis of V_HY101F appears straightforward since there is no solvent network directly associated with the hydroxyl group of V_HTyr101 in the complex interface. Truncation to Phe results in an unfavorable $\Delta\Delta H$ of 31 kJ·mol^{-1}. In this case it is clear that two hydrogen bonds are lost, other structural differences compared to WT are small, and $Asp119_{HEL}$ is not left with its hydrogen-bonding potential unsatisfied (see below and Figure 5C). Thus, it is probably valid to assume that most of the $\Delta\Delta H$ component arises from the loss of the two hydrogen bonds. The resulting estimate of the contribution of each hydrogen bond is therefore ∼16 kJ·mol^{-1}. Since hydrogen bonds are essentially electrostatic interactions between atoms of opposite partial charge, the strength of a hydrogen bond depends most critically on the hydrogen bond donor−acceptor distance, the magnitudes of the partial charges on the donor and acceptor atoms, and the local dielectric constant. With regard to the dielectric constant, it is pertinent that the hydrogen bonds between V_HTyr101 and HEL are buried in the interface of the complex while those from V_LTyr50 and V_HTyr32 are on the periphery (Figure 1). Thus, it is possible that the hydrogen bonds from V_HTyr101 are elevated in strength compared to those from V_LTyr50 and V_HTyr32 due to a lower dielectric constant in the protein−protein interface compared to the periphery. However, such an effect is likely to be small since the FvD1.3−HEL interface is predominantly made up of polar residues, is highly solvated, and, therefore, should have a dielectric constant much closer to that of the solvent-exposed surface. It is unlikely that this protein−protein interface has electrostatic properties similar to that of a hydrophobic interior of a folded globular protein where the low dielectric constant would magnify the strength of hydrogen bonds.

It has been noted that the discrepancy between the apparent contribution to ΔG of an interaction (ΔG_{app}) and the intrinsic ΔG—the actual energetic contribution of a particular interaction (ΔG_{int})—may be large when a mutation leaves a charged hydrogen bond donor or acceptor with its hydrogen-bonding potential unsatisfied (Fersht, 1988). This point may be relevant here since three of the hydrogen bonds analyzed in this study involve one charged residue from HEL. As such, it is possible that mutation of the corresponding D1.3 partner in the hydrogen-bonding interaction could have an anomalously large destabilizing effect. Examining each mutant structure with this possibility in mind, it is apparent that in no case is the hydrogen-bonding potential of the charged HEL side chains left unsatisfied. For the V_LY50S−HEL complex, both carboxylate O^{δ} atoms of $Asp18_{HEL}$ are hydrogen bonded to interface solvent molecules (Figure 5A). Likewise, $Lys116_{HEL}$ in the V_HY32A complex is within hydrogen-bonding distance of two water molecules (Figure 5B). Finally, as stated before, $Asp119_{HEL}$ in the V_HY101F complex is involved in an intramolecular hydrogen bond with the backbone nitrogen of $Gln121_{HEL}$ (Figure 5C). Therefore, in all three cases ΔG_{app} and ΔG_{int} should be similar in magnitude. The validity of this reasoning could be tested by double mutant cycles (Serrano et al., 1990, 1991; Schreiber & Fersht, 1995).

The importance of hydrogen bonds in contributing to the affinity and specificity of protein−ligand complex formation has been investigated in several systems. For example, truncation of a side chain in a tRNA synthetase−substrate complex to leave an uncharged, unpaired hydrogen bond donor or acceptor weakened binding by 2−6 kJ·mol^{-1} (Fersht et al., 1985). Truncation of a side chain to leave an unpaired and charged donor or acceptor weakened binding by an additional ∼12 kJ·mol^{-1} (Fersht et al., 1985). In another study, comparison of two thermolysin−inhibitor complexes that were essentially identical except for the presence or absence of a specific hydrogen bond differed in binding energy by 17 kJ·mol^{-1} (Tronrud et al., 1987). Entropy compensation effects cannot be addressed in these studies since only changes in ΔG were measured. However, the decrease in binding affinity (17 kJ·mol^{-1}) observed in the thermolysin−inhibitor system is in close agreement with the estimate of the contribution of a hydrogen bond (31.3/2 ≈ 16 kJ·mol^{-1}) obtained from the analysis of the V_HY101F−HEL complex.

A recent study, comparing the crystal structure of an antibody−HEL mutant complex with the WT structure, concluded that the HEL mutation Arg68Lys results in the net loss of about one interface hydrogen bond (Chacko et al., 1995). The hydrogen-bonding analysis was complicated by the fact that Lys68 in the mutant complex appears to exist in two conformations. This antibody, HyHEL-5, forms a complex with HEL with a K_b of 10^{11} M^{-1} (Padlan et al., 1989). The Arg68Lys lysozyme mutant binds with an ∼1000-fold lower affinity, which corresponds to a $\Delta\Delta G$ of 17 kJ·mol^{-1} (Lavoie et al., 1990). Once again, only values for ΔG were obtained in these experiments; however, if the entropy compensation is small, then the resulting enthalpic contribution of a hydrogen bond is similar to the value we obtained in the V_HY101F system.

The crystal structure of FvD1.3 complexed with turkey egg white lysozyme (TEL) has also been elucidated and shows the same mode of binding as HEL (Braden et al., 1996). However, HEL and TEL differ by one amino acid in the interface ($Gln121_{HEL}$ → $His121_{TEL}$), and K_b for the FvD1.3−TEL reaction is 7.0×10^5 M^{-1}, that is, about 400-fold lower than the FvD1.3−HEL reaction. Differences in ΔG, ΔH, and $T\Delta S$, compared to FvD1.3−HEL are 16 kJ·mol^{-1}, 36 kJ·mol^{-1}, and 22 kJ·mol^{-1}, respectively. The large $\Delta\Delta H$ is not surprising since, in the FvD1.3−HEL complex, the side chain of $Gln121_{HEL}$ forms two hydrogen bonds to the backbone of FvD1.3 plus one hydrogen bond to the aromatic ring of V_LTyr32. Moreover, Gln121 shows good shape complementarity to a pocket formed by the aromatic side chains of V_LTyr32, V_LTrp92, and V_HTyr101 and makes van der Waals contacts with these residues. When Gln121 is effectively substituted by His in the FvD1.3−TEL complex, a conformational change in D1.3 takes place in order to accommodate the His side chain. This conformational change—a peptide flip at V_L residues 92 and 93—enables His121 to form one hydrogen bond with D1.3. Thus, a total of two interface hydrogen bonds are lost. However, the contribution of the hydrogen bond from Gln121 to the aromatic ring of V_LTyr32 in the WT complex is difficult to estimate (Levitt & Perutz, 1988; Jamison et al., 1995).

Entropy Compensation. The previous section was limited to a discussion of interactions that may affect the enthalpy of the system, namely, electrostatic (hydrogen bonds in this case) and van der Waals interactions. As noted before, the loss in affinity for all three mutant Fv molecules is smaller than would be expected on the basis of enthalpy considerations alone; that is, entropy compensation is in effect. Entropy compensation is a phenomenon that has been observed in many systems including the D1.3−HEL (Ito et al., 1993) and HyHEL10−HEL binding reactions (Tsumoto et al., 1994). Since all of the crystal structures presented here are isomorphous to the wild-type crystal structure, local *B*-factor differences are attributed to the effects of the interface mutations and not to any differences in crystal packing. Of the mutants investigated in this study, entropy compensation is greatest for V_HY101F. Increases in solvent and protein motion, as indicated by the crystallographic *B*-factors (Table 4), must contribute to the entropy compensation observed for the other two mutants. However, for the V_HY101F complex there are no changes in solvent structure or *B*-factors. Here, the most plausible explanation lies in the differing entropy of the unbound WT and V_HY101F Fv molecules. Of relevance to this point is the observation that the mean *B*-factor of V_HTyr101 in the unbound WT Fv is 80% larger than in the complex. As argued by Bhat et al. (1994), this quenching of side chain mobility upon complex formation is entropically unfavorable for binding. Using similar reasoning, an explanation for the observed entropy compensation for the V_HY101F−HEL reaction is that the mobility of V_HPhe101 in the unbound Fv is much closer to its mobility in the complex. This hypothesis may be tested by determining the crystal structure of the unbound mutant Fv. An alternative explanation is that the solvent structure around V_HTyr101 in the unbound state differs substantially from that in the Phe mutant, giving rise to a perturbed hydrophobic effect. This is a reasonable possibility considering the contrasting hydrophobicity and hydrogen-bonding potential of tyrosine and phenylalanine. In the unbound WT Fv structure, the V_HTyr101 side chain is hydrogen bonded to one water molecule with a high temperature factor ($B = 45$ Å^2). However, V_HTyr101 also makes contacts with a neighboring FvD1.3 molecule in the crystal, thus complicating any analysis of its structure and energetics in the unbound state.

The above arguments emphasize the potential importance of the unbound structures when attempting to understand the thermodynamic consequences of interface mutations. Although *B*-factor increases and small conformational changes may contribute to entropy compensation in the V_LY50S and V_HY32A systems, exactly the same arguments regarding the structure and energetics of the unbound state also apply in those cases.

Conclusions. Several conclusions may be drawn from this study. The calorimetric and structural data provide strong support for the concept that solvent interactions can make large contributions to the enthalpy of binding and, therefore, to the affinity of protein−protein complexes. Although solvent rearrangements are localized and their effects do not extend beyond the vicinity of the mutation, they are important in two ways. First, water molecules may act as "adaptors" to correct imperfections introduced into the interface by the mutation. Indeed, losses of complementarity in solvent-accessible regions of the interface tend to be compensated by the stable inclusion of additional water molecules rather than by adjustments in protein structure although we do

observe small but significant adjustments in all three structures analyzed here. In another antigen−antibody system, crystallographically defined structural adjustments were suggested as a means of compensating for the effects of mutations (Tulip et al., 1992b). Small structural adjustments predominantly result when mutations are introduced into protein cores (Buckle et al., 1993; Chen et al., 1993; Matthews, 1995), although incorporation of solvent has also been observed (Buckle et al., 1996). Second, the disruption of ordered solvent networks bridging antigen and antibody may contribute significantly to entropy compensation. Increases in the mobility of side chains of residues in proximity to the mutation provide a supplementary mechanism for entropy compensation. Finally, the potential importance of knowing the high-resolution crystal structures of unbound mutants, in addition to crystal structures of the mutants in complexed form, should not be overlooked when attempting to understand the thermodynamic consequences of interface mutations in structural terms.

REFERENCES

Amit, A. G., Mariuzza, R. A., Phillips, S. E., & Poljak, R. J. (1986) *Science 233*, 747−753.

Bhat, T. N., Bentley, G. A., Fischmann, T. O., Boulot, G., & Poljak, R. J. (1990) *Nature 347*, 483−485.

Bhat, T. N., Bentley, G. A., Boulot, G., Greene, M. I., Tello, D., Dall'Acqua, W., Souchon, H., Schwarz, F. P., Mariuzza, R. A., & Poljak, R. J. (1994) *Proc. Natl. Acad. Sci. U.S.A. 91*, 1089−1093.

Bizebard, T., Gigant, B., Rigolet, P., Rasmussen, B., Diat, O., Bosecke, P., Wharton, S. A., Skehel, J. J., & Knossow, M. (1995) *Nature 376*, 92−94.

Bossart-Whitaker, P., Chang, C. Y., Novotny, J., Benjamin, D. C., & Sheriff, S. (1995) *J. Mol. Biol. 253*, 559−575.

Boulot, G., Eisele, J. L., Bentley, G. A., Bhat, T. N., Ward, E. S., Winter, G., & Poljak, R. J. (1990) *J. Mol. Biol. 213*, 617−619.

Braden, B. C., Souchon, H., Eisele, J. L., Bentley, G. A., Bhat, T. N., Navaza, J., & Poljak, R. J. (1994) *J. Mol. Biol. 243*, 767−781.

Braden, B. C., Fields, B. A., Ysern, X., Goldbaum, F. A., Dall'Acqua, W., Schwarz, F. P., Poljak, R. J., & Mariuzza, R. A. (1996) *J. Mol. Biol. 257*, 889−894.

Brünger, A. T. (1992) *X-PLOR Version 3.1. A System for X-ray Crystallography and NMR*, Yale University Press, New Haven and London.

Buckle, A. M., Henrick, K., & Fersht, A. R. (1993) *J. Mol. Biol. 234*, 847−860.

Buckle, A. M., Cramer, P., & Fersht, A. R. (1996) *Biochemistry 35*, 4298−4305.

Bundle, D. R., Baumann, H., Brisson, J. R., Gagne, S. M., Zdanov, A., & Cygler, M. (1994) *Biochemistry 33*, 5183−5192.

Chacko, S., Silverton, E. W., Kam-Morgan, L., Smith-Gill, S. J., Cohen, G., & Davies, D. R. (1995) *J. Mol. Biol. 245*, 261−274.

Chen, Y. W., Fersht, A. R., & Henrick, K. (1993) *J. Mol. Biol. 234*, 1158−1170.

Chilkoti, A., Tan, P. H., & Stayton, P. S. (1995) *Proc. Natl. Acad. Sci. U.S.A. 92*, 1754−1758.

Chitarra, V., Alzari, P. M., Bentley, G. A., Bhat, T. N., Eisele, J. L., Houdusse, A., Lescar, J., Souchon, H., & Poljak, R. J. (1993) *Proc. Natl. Acad. Sci. U.S.A. 90*, 7711−7715.

Clackson, T., & Wells, J. A. (1995) *Science 267*, 383−386.

Colman, P. M., Laver, W. G., Varghese, J. N., Baker, A. T., Tulloch, P. A., Air, G. M., & Webster, R. G. (1987) *Nature 326*, 358−363.

Fersht, A. R. (1988) *Biochemistry 27*, 1577−1580.

Fersht, A. R., Shi, J. P., Knill-Jones, J., Lowe, D. M., Wilkinson, A. J., Blow, D. M., Brick, P., Carter, P., Waye, M. M., & Winter, G. (1985) *Nature 314*, 235−238.

Fields, B. A., Goldbaum, F. A., Ysern, X., Poljak, R. J., & Mariuzza, R. A. (1995) *Nature 374*, 739−742.

Fischmann, T. O., Bentley, G. A., Bhat, T. N., Boulot, G., Mariuzza, R. A., Phillips, S. E., Tello, D., & Poljak, R. J. (1991) *J. Biol. Chem. 266*, 12915−12920.

Goldbaum, F. A., Schwarz, F. P., Eisenstein, E., Cauerhff, A., Mariuzza, R. A., & Poljak, R. J. (1996) *J. Mol. Recognit. 9*, 6−12.

Howard, A. J., Gilliland, G. L., Finzel, B. C., Poulos, T. L., Ohlendorf, D. H., & Salemme, F. R. (1987) *J. Appl. Crystallogr. 20*, 383−387.

Ito, W., Iba, Y., & Kurosawa, Y. (1993) *J. Biol. Chem. 268*, 16639−16647.

Jamison, R. S., Kakkad, B., Ebert, D. H., Newcomer, M. E., & Ong, D. E. (1995) *Biochemistry 34*, 11128−11132.

Kunkel, T. A. (1987) *Methods Enzymol. 154*, 367−382.

Lavoie, T. B., Kam-Morgan, L. N. W., Mallet, C. P., Schilling, J. W., Prager, E. M., Wilson, A. C., & Smith-Gill, S. J. (1990) in *Use of X-ray Crystallography in the Design of Antiviral Agents* (Laver, W. G., & Air, G. M., Eds.) Academic Press, New York.

Lescar, J., Pellegrini, M., Souchon, H., Tello, D., Poljak, R. J., Peterson, N., Greene, M., & Alzari, P. M. (1995) *J. Biol. Chem. 270*, 18067−18076.

Levitt, M., & Perutz, M. F. (1988) *J. Mol. Biol. 201*, 751−754.

Luzzati, V. (1952) *Acta Crystallogr. 5*, 802−810.

Malby, R. L., Tulip, W. R., Harley, V. R., McKimm-Breschkin, J. L., Laver, W. G., Webster, R. G., & Colman, P. M. (1994) *Structure 2*, 733−746.

Matthews, B. W. (1995) *Adv. Protein Chem. 46*, 249−278.

McPhalen, C. A., & James, M. N. G. (1988) *Biochemistry 27*, 6582−6598.

Padlan, E. A., Silverton, E. W., Sheriff, S., Cohen, G. H., Smith-Gill, S. J., & Davies, D. R. (1989) *Proc. Natl. Acad. Sci. U.S.A. 86*, 5938−5942.

Prasad, L., Sharma, S., Vandonselaar, M., Quail, J. W., Lee, J. S., Waygood, E. B., Wilson, K. S., Dauter, Z., & Delbaere, L. T. (1993) *J. Biol. Chem. 268*, 10705−10708.

Sanger, F., Nicklen, S., & Coulson, A. R. (1977) *Proc. Natl. Acad. Sci. U.S.A. 74*, 5463−5467.

Schreiber, G., & Fersht, A. R. (1995) *J. Mol. Biol. 248*, 478−486.

Schwarz, F. P., Puri, K. D., Bhat, R. G., & Surolia, A. (1993) *J. Biol. Chem. 268*, 7668−7677.

Schwarz, F. P., Tello, D., Goldbaum, F. A., Mariuzza, R. A., & Poljak, R. J. (1995) *Eur. J. Biochem. 228*, 388−394.

Serrano, L., Horovitz, A., Avron, B., Bycroft, M., & Fersht, A. R. (1990) *Biochemistry 29*, 9343−9352.

Serrano, L., Bycroft, M., & Fersht, A. R. (1991) *J. Mol. Biol. 218*, 465−475.

Sheriff, S., Silverton, E. W., Padlan, E. A., Cohen, G. H., Smith-Gill, S. J., Finzel, B. C., & Davies, D. R. (1987) *Proc. Natl. Acad. Sci. U.S.A. 84*, 8075−8079.

Tartof, K. D., & Hobbs, C. A. (1987) *Bethesda Res. Lab. Focus 9*, 12.

Thaller, C., Weaver, L. H., Eichele, G., Wilson, E., Karlsson, R., & Jansonius, J. N. (1981) *J. Mol. Biol. 147*, 465−469.

Tronrud, D. E., Holden, H. M., & Matthews, B. W. (1987) *Science 235*, 571−574.

Tsumoto, K., Ueda, Y., Maenaka, K., Watanabe, K., Ogasahara, K., Yutani, K., & Kumagai, I. (1994) *J. Biol. Chem. 269*, 28777−28782.

Tulip, W. R., Varghese, J. N., Laver, W. G., Webster, R. G., & Colman, P. M. (1992a) *J. Mol. Biol. 227*, 122−148.

Tulip, W. R., Varghese, J. N., Webster, R. G., Laver, W. G., & Colman, P. M. (1992b) *J. Mol. Biol. 227*, 149−159.

Ward, E. S., Gussow, D., Griffiths, A. D., Jones, P. T., & Winter, G. (1989) *Nature 341*, 544−546.

Wiseman, T., Williston, S., Brandts, J. F., & Lin, L. N. (1989) *Anal. Biochem. 179*, 131−137.

Ysern, X., Fields, B. A., Bhat, T. N., Goldbaum, F. A., Dall'Acqua, W., Schwarz, F. P., Poljak, R. J., & Mariuzza, R. A. (1994) *J. Mol. Biol. 238*, 496−500.

Zdanov, A., Li, Y., Bundle, D. R., Deng, S. J., MacKenzie, C. R., Narang, S. A., Young, N. M., & Cygler, M. (1994) *Proc. Natl. Acad. Sci. U.S.A. 91*, 6423−6427.

BI961709E